Polymer Journal (2013) 45, 449–456

www.nature.com/pj

ORIGINAL ARTICLE

Effect of carbon fiber on the capillary extrusion behaviors of high-density polyethylene

Hideyuki Uematsu, Nobusuke Horisawa, Tomoya Horikida, Shuichi Tanoue and Yoshiyuki Iemoto

The capillary extrusion behaviors of high-density polyethylene (PE) containing carbon fibers (CF) were investigated from a viewpoint of their rheological properties. For values of CF content ranging from 0 to 5 wt%, the oscillatory moduli of PE slightly increased with CF content. Transient shear flow measurements showed that the steady shear viscosity and first normal stress difference of PE also slightly increased with the addition of CF. Conversely, the strain hardening behaviors of PE were suppressed by CF addition. It was found that CF becomes well dispersed in the PE matrix and that the elongation of the PE chain can be prevented by the presence of CF. The swell ratio of PE, which is the ratio of the diameters of the extrudate and the die, decreased with CF. Using a wide entrance angle die, PE/CF exhibited helical distortion at a higher output rate than that of PE. Using a narrow entrance angle die, sharkskin failure was observed in PE/CF at a higher output rate than in PE, although the helical distortion of PE was inhibited by CF. We discuss the origin of the helical distortion as an effect of CF on the swell behavior and the flow instabilities of PE in reference to the rheological behavior.
Polymer Journal (2013) **45,** 449–456; doi:10.1038/pj.2012.167; published online 19 September 2012

Keywords: carbon fiber; flow instability; helical distortion; rheology; swell

INTRODUCTION

In polymer or food extrusion processes, the appearance and properties of the extruded materials depend on the throughput conditions. The diameter of the extruded material is larger than that of the die at low extrusion rates. This behavior, called extrudate swell or the Barus effect, is one of the important viscoelastic responses of polymer melts because this behavior has a key role in the processability of polymers in the extrusion process. Numerous theoretical[1–4] and experimental studies[5–7] on extrudate swell have been conducted. It is well understood from the previous work that the elastic component has a very significant effect on the extrudate swell because the extruded material expands via elastic recovery at the die exit. At the same time, flow instabilities, which are categorized by surface failure and volume distortion, often occur at relatively high extrusion rates. The term 'melt fracture' has been used to describe all types of extrudate distortions. Surface and volume distortions have been classified by various descriptive terms via visual inspection, such as orange peel, sharkskin, screw threaded, helical, and gross (chaotic). The transparency and mechanical properties of the extruded materials degenerate with increasing flow instabilities because their surfaces become irregular. The mechanisms of flow instability have also been extensively investigated. The origin of the surface failure known as sharkskin is an abrupt change in the boundary condition of the tensile deformation near a die exit, which causes sudden stretching of the surface layer of melt.[8,9] In another explanation of surface failure, the slip between the molten polymer and the surface of the die causes the surface failure.[10–15] It is well known that surface failure can easily be observed in polyethylene (PE) containing a high elastic component.[10,14] In contrast, it has been recognized that volume distortion develops due to flow instability at the die entrance.[15–17] Volume distortion can easily develop in polymer systems containing long-chain branches and high molecular weight components.[18–20] In these reports, surface distortion and both helical and chaotic volume distortions were observed with an increase in volumetric flow rate (shear rate), depending on various factors, such as the die geometry, material and so on. Sometimes the surface failure and helical distortion were not apparent. It is especially difficult to observe the helical distortion in a limited range of extrusion rates. Meller *et al.*[19] have explained the development of volume and surface distortion via the relationship existing between the extensional stress at the die entrance and the shear stress at the die wall. The instability at the die entrance or wall therefore appears above the critical extensional or shear stress. Thus, it is suggested that the swelling phenomenon and flow instability may be controlled by the elastic component. However, the properties (for example, strength) of extruded materials at room temperature would decrease if the elastic component were reduced to prevent the swelling phenomenon and flow instability. Therefore, from the industrial point of view, it is necessary to determine methods to control the extrusion behavior without reducing the elastic component.

Polymeric materials are often combined with other materials to add new functionality to the end products. Great attention has been given

Fiber Amenity Engineering, Graduate School of Engineering, University of Fukui, Bunkyo, Fukui, Japan
Correspondence: Dr H Uematsu, Fiber Amenity Engineering, Graduate School of Engineering, University of Fukui, 3-9-1 Bunkyo, Fukui 910-8507, Japan.
E-mail: uematsu@matse.u-fukui.ac.jp
Received 14 May 2012; revised 25 June 2012; accepted 2 July 2012; published online 19 September 2012

to the use of nano-size additives in creating materials with enhanced properties, for example, clay with a higher modulus and carbon nanotubes (CNT) with greater electrical and thermal properties than polymers. Recently, vapor-grown carbon fiber (CF) (that is, VGCF) was created as a new class of CF that is distinct from other types of CFs in its production method.[21] VGCF has been industrially focused because the productivity of VGCF is higher than that of CNTs. The structure of VGCF exhibits excellent electrical conductivity, thermal conductivity, strength, lubricity and resiliency because of a high degree of graphitization.[22,23] As filler dispersion influences composite properties, many properties of composites containing clay or VGCF have naturally been reported in terms of the filler dispersion.[24–28] Yet, it is necessary to study the extrusion behavior of the composite for polymer extrusion processing, because the swelling phenomenon and flow stability are directly linked to the processability. Few studies have examined the extrusion behavior of polymer composites. It has been reported that the swelling phenomena of molten polymer was reduced by the addition of clay and that the decrease in the swell ratio, the ratio of the diameter of the extruded material to that of the capillary die, could be attributed to the reduced elastic recovery.[29–31] The large reduction of swelling phenomena was also reported in the composite containing a network structure of silica particles.[32] The effects of CNT and CF, which are, respectively, micro- and millimeter in length, on the die swell of molten polymer are noteworthy because the swelling behavior drastically varied with the length of the additive.[33–35] When a high aspect ratio CF was added, the swell of polymer/CF was larger than that of polymer at a high extrusion rate, although the opposite result was shown at low extrusion rates.[33] In contrast, die shrinkage was observed in the composite containing high aspect ratio CNT.[34] Many results have been discussed for composites with high entanglement and/or contact with CNT or CF. The swell behavior of molten polymer with a high dispersion state of CNT or CF has scarcely been studied. Moreover, flow instabilities have barely been investigated within polymer composite systems. Studies on the extrusion behavior, such as die swell and flow instability, of polymer/CNT or polymer/CF are necessary for processing operations.

In this study, the effects of relatively small and low aspect ratio CF on the extrusion behavior of PE were investigated using a capillary rheometer. Notably, we focused on the development of helical distortion and discussed the origin of helical distortion in terms of the rheological behavior via the effect of CF on the swell and flow instabilities of PE.

EXPERIMENTAL PROCEDURES

Materials

The polymer used in this study was high-density PE (Japan Polyethylene Corporation, Tokyo, Japan, HD230) with a relative density of 0.946, a melt index of 0.9 g per 10 min, $M_w = 140\,kg\,mol^{-1}$ and a molecular distribution of 12.5. VGCF made by Showa Denko KK, Japan was used as a CF. The average diameter and length of the CFs were 150 nm and 6 μm, respectively. PE was compounded with CF in a co-rotating twin screw extruder (S1 KRC kneader, Kurimoto, Ltd., Osaka, Japan), and the mixed samples were pelletized. The screw diameter and the ratio of screw length to diameter were 25 mm and 10.2, respectively. The barrel temperature and screw rotation speed were, respectively, set at 200 °C and 150 r.p.m. The content of CF varied from 0 to 5 wt%. For example, the composite containing 5 wt% CF is denoted by PE/CF5 in this study. PE/CF composite pellets were compression-molded into disks with 25 mm diameters and 0.5–1.0 mm thicknesses for use as dynamic rheological test specimens and into rectangular bars of 15 mm in length, 5 mm in width and 0.5 mm in thickness to measure the uniaxial elongational viscosity. A mold containing the composite pellets was placed in a surrounding environment of 200 °C for 5 min to allow the pellets to melt. After 5 min, the pressure was gradually applied and then held for 5 min to set the shape of the samples. The molded samples were cooled at room temperature for 10 min. The melt flow behaviors were investigated using PE/CF pellets.

Measurements

Dynamic rheological measurements of PE/CF were performed at various temperatures T from 130 to 200 °C with a strain-controlled rheometer (ARES, TA Instruments, Tokyo, Japan). The parallel plates of 25 mm in diameter were used for the frequency ω sweeps. The gap between parallel plates was approximately 0.5 mm. The ω dependencies of the storage and loss moduli G' and G'' were measured in the ω range from 0.1 to 100 rad s^{-1}. The strain ranged from 0.01 to 0.2 in the linear viscoelastic criterion for PE composites. The steady shear viscosity η_s and first normal stress difference N_1 were measured in transient shear flow mode at 200 °C across a range of shear rates from 0.1 to 1.0 s^{-1}. Rheological measurements were performed without thermal degradation during the frequency sweep tests. Measurements of the uniaxial elongational viscosity η_E at constant strain rate $\dot{\varepsilon}$ were carried out with ARES using the elongational viscosity mode at 200 °C. The values of $\dot{\varepsilon}$ varied from 0.01 to 1.0 s^{-1}.

The melt flow behavior in the capillary extrusion was investigated at 200 °C by the capillary rheometer (CFT-500D, Shimadzu Corporation, Kyoto, Japan) to evaluate the appearance of extrudates. The illustration of the capillary rheometer is shown in Figure 1. The barrel diameter D' was 10 mm, and the circular die with $L/D = 10/1$ (mm) was employed. Two types of dies with different entrance angles θ of 180° and 90° were used. PE/CF composite pellets were melted in a barrel for 10 min; the volumetric flow rate was then measured at a constant load. The flow behaviors of PE/CF were investigated at various loads. The shear rate and shear stress on the die wall of a circular die were calculated from the volumetric flow rate and the load, respectively.

RESULTS AND DISCUSSION

Linear viscoelasticity and transient shear viscosity

The storage moduli G' at various temperatures T were superimposed onto a master curve by shifting along the ω axis regardless of the CF content. The loss moduli G'' were similarly superimposed onto a master curve by shifting along the ω axis. Figures 2a and b, respectively, show the master curves of G' and G'' of PE/CF. The reference temperature T_r was 200 °C. Figure 3 shows the shift factor a_T for the composite and the matrix used to construct the master curves. As shown in Figure 2, G' and G'' of PE slightly increased with CF content. The slopes of G' and G'' were independent of the content of CF and, respectively, approached 2 and 1 at low frequencies. Moreover, as observed in Figure 3, the temperature dependence of a_T was almost the same irrespective of the CF content. It should be emphasized that the viscoelastic properties of PE/CF obey the time-temperature superposition and that the temperature dependences of

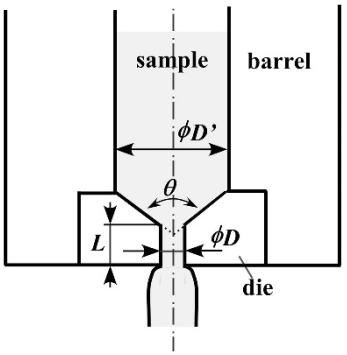

Figure 1 Schematic diagram of the apparatus used to investigate the extrusion behavior of PE/CF. A full color version of this figure is available at *Polymer Journal* online.

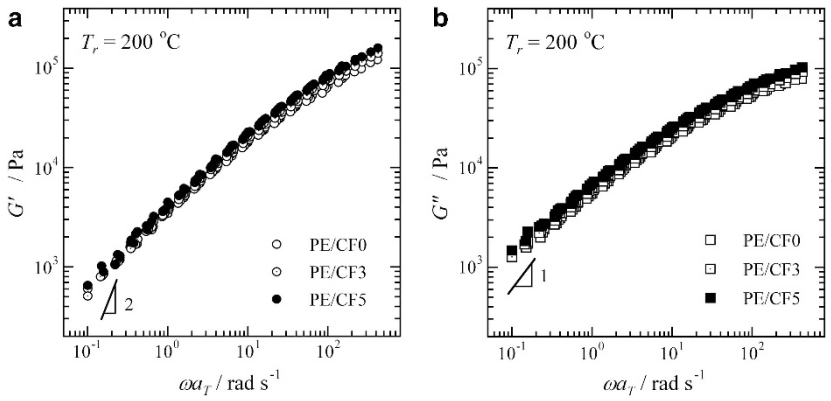

Figure 2 Master curves of (**a**) storage modulus G' and (**b**) loss modulus G'' plotted against angular frequency ω for PE/CF at 200 °C.

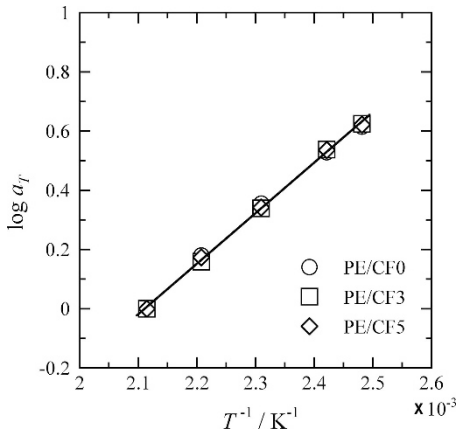

Figure 3 Temperature dependence of the shift factor a_T plotted against T^{-1} for PE/CF.

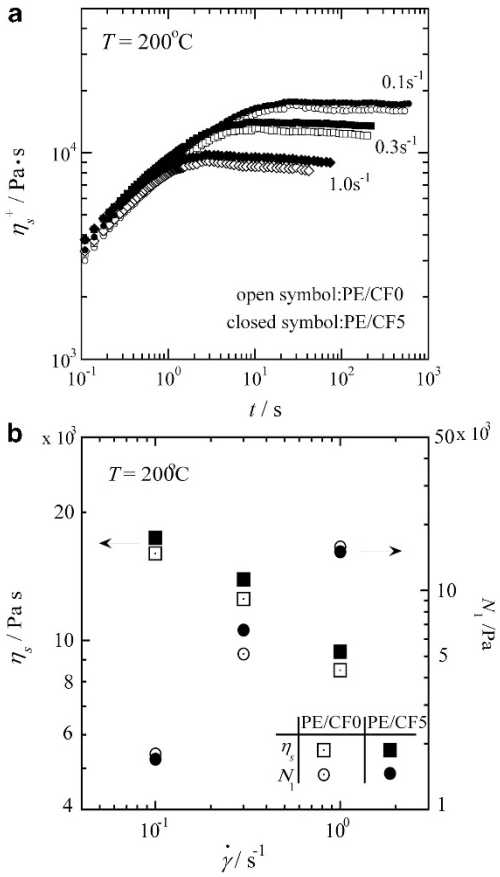

Figure 4 (**a**) Transient shear viscosity η_s^+ against time t and (**b**) first normal stress difference N_1 against shear rate $\dot{\gamma}$ of PE/CF0 and PE/CF5 at shear rates 0.1–1.0 s^{-1} at 200 °C.

a_T were identical. These data indicate that the dispersion state of CF in the matrix does not change with T and that the behavior of CF is governed by the friction from the PE matrix. Thus, PE/CF does not include an agglomerate structure of CF, and the PE chain hardly absorbs on the CF surface at each T.

In Figure 4a, we show the transient shear viscosity η_s^+ of PE/CF0 and PE/CF5 via the increasing shear flow across the constant shear rate range of 0.1–1.0 s^{-1}. The value of η_s^+ for PE slightly increased with CF at each shear rate $\dot{\gamma}$. The steady shear viscosity η_s and the normal stress difference N_1 were shown as a function of $\dot{\gamma}$ in Figure 4b. The η_s of PE/CF gradually decreased with increasing $\dot{\gamma}$, irrespective of CF content. Thus, similar shear thinning was observed in PE/CF. The value of N_1 for PE/CF5 is nearly equivalent to that of PE/CF0. The empirical Cox–Merz rule[36] states that complex viscosity η^* versus the dynamic frequency ω obtained from small-amplitude oscillatory shear is numerically equal to η_s versus $\dot{\gamma}$. This principle is widely successful in describing the observed behavior of isotropic polymeric solutions and polymer melts, although there is no theoretical explanation for such a relationship. In our system, the Cox–Merz rule holds, irrespective of CF content. Miyazono *et al.*[37] reported on the relationship between the morphology and rheological behavior of polymer composites containing well-dispersed CF. In this study, the well-dispersed CF rotated in shear flow without orientation and the Cox–Merz rule was realized. The shear rheological behavior in PE/CF is typical for systems with well-dispersed fiber.

Uniaxial elongational viscosity

Figures 5a and b show the uniaxial elongational viscosity η_E^+ of PE/CF0 and PE/CF5, respectively, for various strain rates $\dot{\varepsilon}$ at 200 °C. In these figures, the solid lines indicate 3η, which is the shear stress growth function in the linear viscoelastic region, as calculated from G' and G'' using an approximate equation proposed by Osaki *et al.*[38] The linear elongational viscosity, which is independent of $\dot{\varepsilon}$, is generally found to be in agreement with the calculated curve of 3η; this relationship is referred to as Trouton's rule.[39] The steep increase of η_E^+ above 3η is called strain hardening. It is well known that strain hardening can develop with the extension of the polymer chain.[40,41] Strong strain

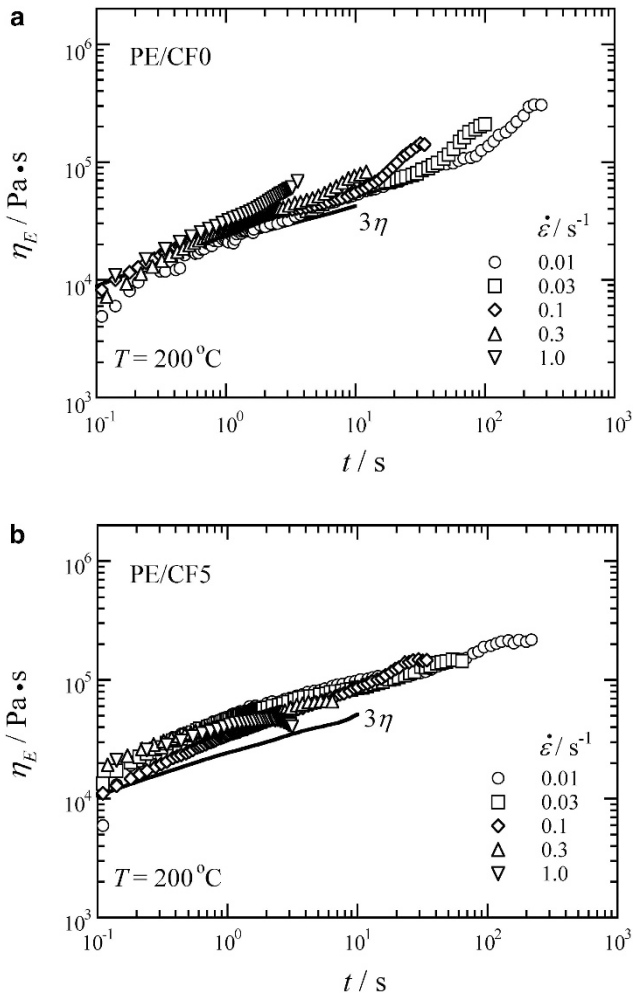

Figure 5 Time dependence of uniaxial elongational viscosity η_E^+ at various strain rates $\dot{\varepsilon}$ for (**a**) PE/CF0 and (**b**) PE/CF5 at 200 °C. The solid lines represent 3η of PE/CF0 and PE/CF5 calculated from dynamic viscoelastic data.

hardening is observed in polymer systems containing long branched chains,[42,43] high molecular weight components[44,45] and so on.

The η_E^+ of PE/CF0 followed the linear viscoelastic function 3η over the entire time scale measured. Strain hardening was shown in the PE/CF0 system. It is likely that strain hardening was observed because the high molecular weight component (the effect of broad molecular distribution) was included, as in previous reports.[44,45] In contrast, the elongational viscosities of PE/CF5 almost coincided over the entire time scale measured, irrespective of $\dot{\varepsilon}$. In other words, a steep increase in η_E for PE/CF5 could hardly be observed. Compared with the linear elongational viscosity and the function 3η, as calculated from the dynamic viscoelasticity of PE/CF5, the linear elongational viscosity was 4–5 times as large as 3η.

Trouton's ratio, which is the ratio of linear elongational and shear viscosities ($TR = \eta_E/3\eta$), agreed with the calculated values for the shape and content of fiber in a well-dispersed system. The equation was proposed by Batchelor (Batchelor's theory).[46] The well-known formula in polymer mixtures containing anisotropic fiber is shown as:

$$TR = \frac{4\phi(l/d)^2}{3\ln(\pi/\phi)} \quad (1)$$

where ϕ is the volume fraction of fiber, l is the length and d is the diameter of the fiber.[46–48] In this equation, there are two assumptions: the value of l is much greater than the distance h among fiber, h is much larger than d, namely ($d \ll h \ll l$). Miyazono *et al.*[37] reported that Batchelor's equation can be applied in a molten polymer composite by calculating the number average length. We reported that the number average length of CF decreased by 60–70 percent when mixed with a co-rotating twin screw extruder, irrespective of CF content.[49] When it was assumed that the average length of CF decreased by 60–70 percent, the values of TR calculated from equation (1) were 3.8–5.1. Therefore, CF may be well dispersed in the PE matrix, given that the experimental data approximately coincided with Batchelor's theoretical equation. Miyazone *et al.*[37] also explained that the linear elongational viscosity did not agree with 3η, owing to the orientation of the fiber experiencing extensional deformation. In contrast, in the report of Takahashi *et al.*,[50] the strain hardening of these composites became weaker than that of the matrix with fillers of increasing aspect ratios. Strain hardening of polypropylene was suppressed irrespective of the orientation of the glass fiber from the result of Ferec.[51] The streamline can be jumbled by the presence of fiber in the elongational flow field.[52] Therefore, in the extensional deformation field, the extension of the PE chain was suppressed by the presence of CF, irrespective of its orientation. In other words, the elastic components developed in extensional flow were decreased by CF.

Capillary extrusion

The flow characteristics of PE/CF0 and PE/CF5 measured by the capillary rheometer, using an entrance angle of 180° at 200 °C, are shown in Figure 6a. Figure 6b shows the photographs of PE/CF0 and PE/CF5 extrudated at various apparent shear rates $\dot{\gamma}_{ap}$, which is the shear rate on the die wall, assuming a Newtonian fluid. As the molten PE behaves as a non-Newtonian fluid, the value of $\dot{\gamma}_{ap}$ requires correction via the Rabinowitch equation. It is also necessary to correct the apparent shear stress τ_{ap}, which is the shear stress on the wall that accounts for the pressure drops at the die entrance and exit. In this study, the extrusion behavior of PE/CF is discussed with uncorrected data to convey a rough indication. As observed in Figure 6a, the viscosity of PE was scarcely affected by CF at a high strain rate. From Figure 6b, the diameters of the extruded PE/CF0 and PE/CF5 increased with shear rate on die wall, and the cylindrical extrudates adopted orderly spiral, screw-like structures above 1700 and 2500 s^{-1}, respectively. The typical swelling phenomena and flow instability, such as helical distortion, were observed in the PE and PE/CF systems. First, we focus on the effect of CF on the swelling phenomena of PE.

In Figure 7, the swell ratio, which is defined as the ratio of the diameter of the extrudate to that of the die, was plotted as a function of the apparent shear rate $\dot{\gamma}_{ap}$ on the die wall. The swell of PE and PE/CF increased with $\dot{\gamma}_{ap}$. The swell of PE/CF was smaller than that of PE regardless of their equivalent $\dot{\gamma}_{ap}$ values. Figure 8 shows the effect of CF content on the swell of PE and PE/CF at various apparent shear rates. The vertical axis is the swell ratio of PE/CF normalized by the swell ratio SR_{PE} of the PE matrix. The ideal value SR_{ideal} calculated from SR_{PE} and the content ϕ [vol%] of CF using equation(2) was presented in Figure 8 to confirm the volume reduction effect on PE caused by the addition of CF, given that the CF component hardly swells.

$$SR_{ideal} = SR_{PE} \times (1 - \phi/100) \quad (2)$$

As observed in Figure 8, SR_{ideal} decreased with the volume reduction of PE; moreover, the drastic decrease was actually

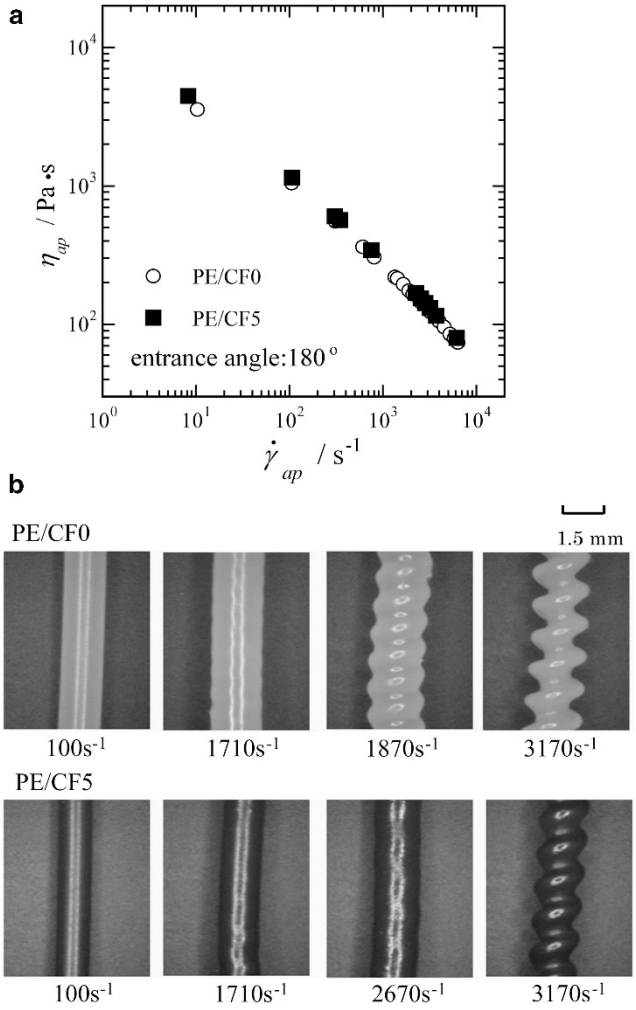

Figure 6 (**a**) Flow characteristic and (**b**) photographs of extruded samples of PE/CF0 and PE/CF5 using a die with an entrance angle of 180° at various apparent shear rates, held at 200 °C.

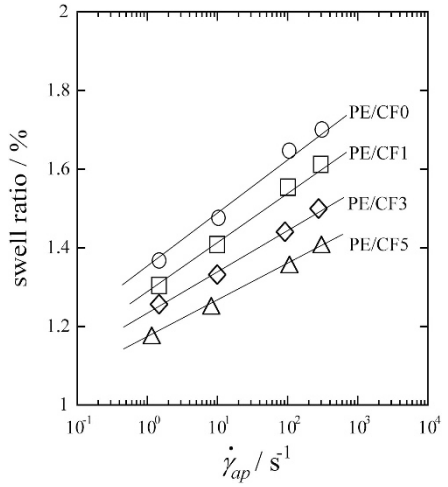

Figure 7 Swell ratio (%) of PE/CF as a function of (**a**) apparent shear rate $\dot{\gamma}_{ap}$, usinga die with an entrance angle of 180° at 200 °C.

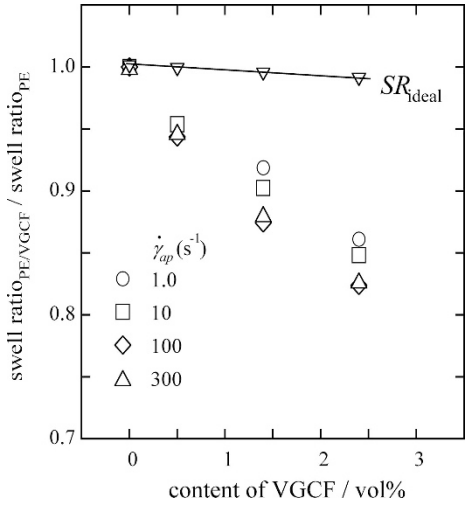

Figure 8 Swell ratio of PE/CF normalized by the swell ratio of PE as a function of the CF content. The solid line SR_{ideal} represents the calculation line using $SR_{ideal} = SR_{PE} \times (1 - \phi/100)$, where SR_{PE} and ϕ are, respectively, the swell ratio of PE and the volume fraction of CF using a die with an entrance angle of 180°.

confirmed in the PE/CF system. In addition, the swell of PE monotonically reduced with increasing CF content, and the reduction effect was promoted with increasing $\dot{\gamma}_{ap}$. Therefore, we found that the decrease in swelling phenomena in the PE/CF system is the result not only of volume reduction of PE but also of the reduction owing to rheological properties.

When the molten polymer extrudes from the exit of die, the extrudate expands because the normal stress is released at the die exit. In other words, the swelling phenomenon is a parameter related to the melt elasticity and occurs as a result of the recovery of the elastic deformation imposed on the capillary. The normal stress difference N_1, which is an index of elasticity in shear flow, was barely altered by the addition of CF at a low shear rate, as shown in Figure 4; however, the swell of PE/CF was smaller than that of PE. These results have been reported in polymer/fiber systems.[33–35,52,53] Jonathan *et al.*[54] have reported that the extensional flow, which is an accelerated flow, is developed in the contraction area located between the reservoir and the capillary. Therefore, the strain hardening, an elastic property at the entrance of the capillary die, is a dominant factor with respect to the swelling behavior. From the results of Figures 4 and 5, it is suggested that the extension of the PE chain was prevented around CFs because the strain-thickening phenomenon shown in the case of PE disappears in the PE/CF system. It is likely that the decreasing swell of PE/CF may be attributed to the reduction of the elastic properties arising from the extensional PE chain.

Volume distortion was shown at high shear rates. The shear stress increased smoothly with shear rate without an inflection point in PE/CF, as shown in Figure 6a. The failures on the surface were observed locally above 600 s^{-1} in the PE system. Moreover, the extrudates completely adopted spiral conformations above 1700 s^{-1}, and the pitch and thread of the screw increased with $\dot{\gamma}_{ap}$, as shown in Figure 6b. The lengths of the non-smooth region of the extrudate, called the unstable length, were measured below 1700 s^{-1} to clarify

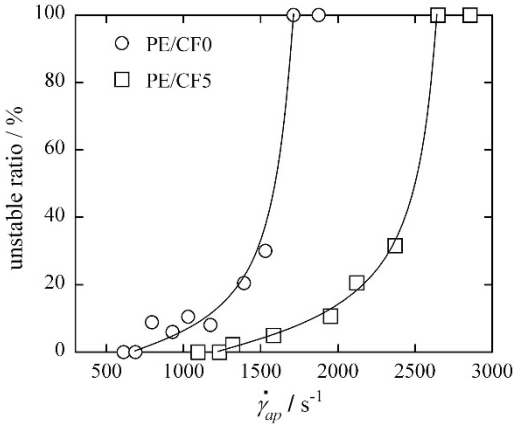

Figure 9 The unstable ratio as a function of the apparent shear rate $\dot{\gamma}_{ap}$ for PE/CF0 and PE/CF5, using a die with an entrance angle of 180° at 200 °C.

the stable-unstable transition region. The non-smooth region of the extrudate was judged by touch. The ratio of the unstable length to the total length, which is called the unstable ratio, is plotted as a function of apparent shear rate in Figure 9. In the region from 600 to 1500 s^{-1}, the stable flow gradually changed to unstable flow with increasing $\dot{\gamma}_{ap}$ in the PE system. However, the unstable ratio drastically increased above 1500 s^{-1}. Therefore, the absolute helical extrudate developed in the narrow region of shear rate above 1500 s^{-1}. In the case of PE/CF5, local and general unstable flows were observed above 1200 and 2600 s^{-1}, respectively. Thus, the stable-unstable transition region in the PE/CF system was also confirmed and significantly shifted to a higher shear rate region than that of PE. Therefore, helical distortion can be prevented with CF. We defined the critical apparent shear rate and shear stress, where the extrudate becomes perfectly helical, as $\dot{\gamma}_{ap\_sp}$ and τ_{ap_sp}, respectively. The values of $\dot{\gamma}_{ap\_sp}$ (a) and τ_{ap_sp} (b) were plotted as a function of the CF content in Figure 10. The turning point shifted to a higher shear rate and stress region with increasing CF content. The result leads to our presumption that the development of helical distortion cannot be explained in terms of shear stress and rate in the die. It is suggested that the helical distortion can be attributed to the unstable flow at the entrance of die.

A corner vortex was formed at the entrance of the die because of the reduced extensional stress at the die entrance. Therefore, the corner vortex develops with increasing volumetric flow rate.[55,56] The flow behavior at the die entrance can be stabilized by the development of the corner vortex; conversely, flow instability is caused by disturbances to the corner vortex. The behavior of the amphibolic flow, which arose temporarily as a stream from the corner vortex to the die, was observed visually at the die entrance by Bagley *et al.*[55] They also reported that the size of the corner vortex gyrated with time at constant volumetric flow rates. As the screw-like extrudate was observed at high strain rates, it is reasonable to assume that amphibolic flow also developed at the die entrance in our system. The size of the extrudate diameter, which is the length between berms and swales, decreased with the strain rate, irrespective of the CF content above $\dot{\gamma}_{ap\_sp}$. This result implied that the elastic component at the die entrance might be inhibited by the development of amphibolic flow. With regard to the rheological behavior of PE/CF, the addition of CF caused the strain hardening to decrease while causing the elongational stress to increase. Although the magnitude of the elongational stresses of PE/CF0 and PE/CF5 almost coincided and the elongational stress of PE/CF5 was larger than that of PE/CF0, the

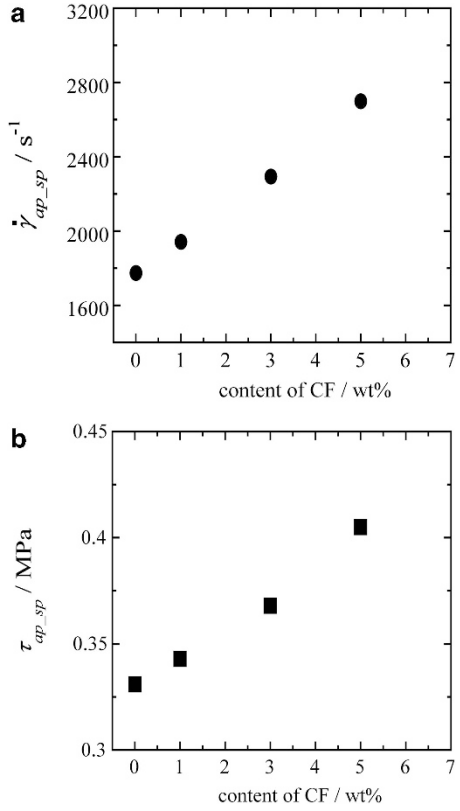

Figure 10 Relationship between (**a**) critical apparent shear rate $\dot{\gamma}_{ap\_sp}$ and (**b**) stress τ_{ap_sp} and the CF content using a die with an entrance angle of 180°.

elastic component in PE/CF5 at the die entrance was less than that in PE/CF0. These results indicate that the flow can be stabilized by reduction of the elastic component at the die entrance with the addition of CF. Therefore, an amphibolic flow may develop to compensate for the elastic component at the die entrance, and a helical distortion appears as a result.

To confirm the effect of the die entrance on the helical distortions of PE/CF0 and PE/CF5, the extrusion behavior was investigated using an entrance angle of 90°. Photographs of the extrudates of PE and PE/CF5 are shown in Figure 11. The stable-unstable transition region was narrow and the cylindrical extrudate was converted to an absolute spiral extrudate above $\dot{\gamma}_{ap} = 7000\,s^{-1}$ for PE/CF0. In the case of PE/CF5, surface failures were observed above 10 000 s^{-1}. Compared with the results of Figure 9 (employing an entrance angle of 180°), helical distortion was difficult to develop using a die with a narrow entrance angle of 90°. This result implied that the formation of an amphibolic flow was prevented by the stabilization of flow in the convergent entrance. Therefore, we considered that the unstable flow was difficult to generate because the elongational flow can be developed gradually in the convergent entrance. In other words, it was qualitatively found that the flow at the die entrance can be stabilized by the presence of CF. Moreover, the non-smooth surface was developed in the PE/CF5 system. The shear stress of PE/CF5 increased monotonically with the strain rate, irrespective of the appearance of surface failure. Thus, the surface failure known as sharkskin was observed in PE/CF5. It is well known that this surface failure occurs due to slip between the surface of the die and the molten polymer,[10–15] and the inflection point in the stress-strain rate curve on the die wall is the result of slip. However, a smooth stress-strain rate curve was observed in PE/CF5. This result

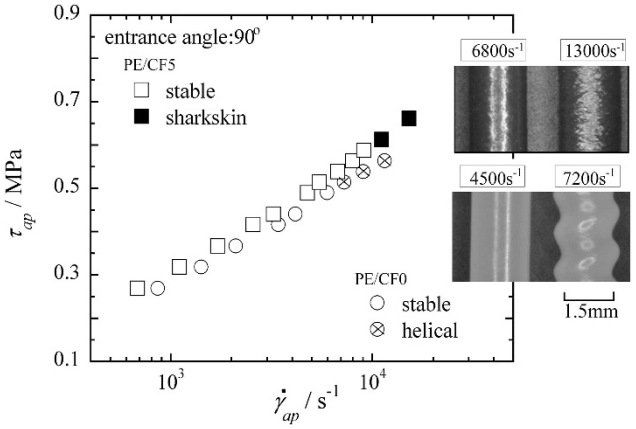

Figure 11 Apparent shear stress plotted against apparent shear rate for PE/CF0 and PE/CF5, using a die with an entrance angle of 90° at various apparent shear rates, held at 200 °C. The photographs present the extrudate for PE/CF0 (white color) and PE/CF5 (dark color) at various apparent shear rates.

led to our presumption that the surface crack was created by an abrupt change in the boundary condition of tensile deformation near a die exit, which caused sudden stretching of a surface layer on the die wall. It is probable that the sharkskin failure developed as a result of discontinuous flow, such as slip at the die exit. The effects of CF on the sharkskin phenomena will be examined in future work.

CONCLUSION

We investigated the effect of CF on the capillary flow behavior of high-density PE in terms of the rheological properties of PE composites with various CF content (0–5 wt%). The storage modulus G' and loss modulus G'' of PE slightly increased with CF content. The temperature dependence of the G' and G'' of PE could not be observed for every CF content. From the linear viscoelasticity results, it was found that CF dispersed easily in the PE matrix. The steady shear viscosity η_s and the normal stress difference N_1 of PE slightly increased with CF content. The empirical Cox–Merz rule held, irrespective of the CF content. The elongational viscosity behavior of PE followed the linear viscosity growth function 3η and exhibited strain hardening. Conversely, the linear elongational viscosity of PE/CF was larger than 3η, and the strain hardening of PE was suppressed by the addition of CF to PE. Comparison with the linear elongational viscosity and 3η using Batchelor's theory suggests that CFs became well dispersed without contacting the PE matrix. The presence of CF was found to have a significant effect on the reduction of the die swell of PE. We found that the decrease in the swell of PE/CF can be attributed to the reduction of elastic properties arising from the extensional PE chain at the die entrance. In cases where a wide entrance angle was used, a helical distortion of the PE composite was also observed for higher shear rates than for those of the PE matrix. In other words, CF could prevent the helical distortion of PE, although the elongational and shear stress increased with CF content. Moreover, the helical distortion of PE transformed into a surface failure with the addition of CF, when a narrow entrance angle was used. It should be emphasized that the flow behavior in the die entrance region could be stabilized by adding CF. We summarize that the helical distortion can be effectively controlled with the addition of a small amount of CF, because helical distortion develops to compensate for the elastic component at the die entrance.

ACKNOWLEDGEMENTS

The authors express their thanks to Mr Takaaki Hattori of the Japan Polyethylene Corporation for the supply of PE samples and for his useful advice.

1 Tanoue, S. & Iemoto, Y. Effect of die gap width on annular extrudates by the annular extrudate swell simulation in steady-states. *Polym. Eng. Sci.* **39,** 2172–2180 (1999).
2 Kajiwara, T., Tomiyama, H., Sueyoshi, Y., Yamamura, M. & Adachi, K. Numerical Simulation of Extrudate Swell Problem and Evaluation of Applicability of Viscoelastic Constitutive Models. 1. A Study on Axisymmetric Extrudate Swell from a Straight Die. *Nihon Reoroji Gakkaishi (J. Soc. Rheol. Jpn.)* **29,** 47–52 (2001).
3 Tanner, R. I. A theory of die-swell revisited. *J. Non-Newtonian Fluid Mech.* **129,** 85–87 (2005).
4 Mu, Y., Zhao, G. & Zhang, C. Numerical Investigation of Die Geometry Effect on LDPE Annular Extrudate Swell. *J. Appl. Polym. Sci.* **117,** 91–109 (2010).
5 Chen, Y. Z. & Li, H. L. Effect of ultrasound on the viscoelasticity and rheology of polystyrene extruded through a slit die. *J. Appl. Polym. Sci.* **100,** 2907–2911 (2006).
6 Song, M. S., Hu, G. X., Yang, Z. H., Xu, Q. & Wu, S. Z. Dynamics of polymeric fluids. 1. The molecular theory of die swell: a set of equation on swelling ratio in extrudates. *J. Mater. Sci. Technol.* **22,** 93–107 (2006).
7 Liang, J. Z. Effects of extrusion conditions on melt viscoelasticity during capillary flow of low-density polyethylene. *J. Thermoplastic Compo. Materials* **22,** 99–110 (2009).
8 ElKissi, N., Paiu, J. M. & Toussaint, F. Sharkskin and cracking of polymer melt extrudates. *J. Non-Newtonian Fluid Mech.* **68,** 271–290 (1997).
9 Rutgers, R. P. G. & Mackley, M. R. The effect of channel geometry and wall boundary conditions on the formation of extrusion surface instabilities for LLDPE. *J. Non-Newtonian Fluid Mech.* **98,** 185–199 (2001).
10 Ramamurthy, A. V. Wall slip in viscous fluid and influence of materials of construction. *J. Rheol.* **30,** 337–358 (1986).
11 Ghanta, V. G., Riise, B. L. & Denn, M. M. Disappearance of extrusion instabilities in brass capillary dies. *J Rheol.* **43,** 435–442 (1999).
12 Rodriguez-Gonzalez, F., Perez-Gonzalez, J., Marin-Santibanez, B. M. & de Vargas, L. Kinematics of the stick-slip capillary flow of high-density polyethylene. *Chem. Eng. Sci.* **64,** 4675–4683 (2009).
13 Rodriguez-Gonzalez, F., Perez-Gonzalez, J., de Vargas, L. & Marin-Santibanez, B. M. Rheo-PIV analysis of the slip flow of a metallocene linear low-density polyethylene melt. *Rheol. Acta.* **49,** 145–154 (2010).
14 Mieda, N. & Yamaguchi, M. Flow instability for binary blends of linear polyethylene and long-chain branched polyethylene. *J. Non-Newtonian Fluid Mech.* **166,** 231–240 (2011).
15 Legrand, F. & Piau, J. M. Spatially resolved stress birefringence and flow visualization in the flow instabilities of a polydimethylsiloxane extruded through a slit die. *J. Non-Newtonian Fluid Mech.* **77,** 123–150 (1998).
16 Wassner, E., Schmidt, M. & Munstedt, H. Entry flow of a low-density-polyethylene melt into a slit die: An experimental study by laser-Doppler velocimetry. *J. Rheol.* **43,** 1339–1353 (1999).
17 Nigen, S., ElKissi, N., Piau, J. M. & Sadun, S. Velocity field for polymer melts extrusion using particle image velocimetry stable and unstable flow regimes. *J. Non-Newtonian Fluid Mech.* **112,** 177–202 (2003).
18 Yannick, G., Jean-Charles, M., Jean-François, T. & Jacques, G. Molecular structure and gross melt fracture triggering. *J. Non-Newtonian Fluid Mech.* **111,** 175–198 (2003).
19 Meller, M., Luciani, A., Sarioglu, A. & Manson, J. A. E. Flow through a convergence. Part 1: critical conditions for unstable flow. *Polym. Eng. Sci.* **42,** 611–633 (2002).
20 Yamaguchi, M., Todd, D. B. & Gogos, C. G. Rheological properties of LDPE processed by conventional processing machines. *Adv. Polym. Technol.* **22,** 179–187 (2003).
21 Choi, Y. K., Sugimoto, K. I., Song, S. M. & Endo, M. Mechanical and thermal properties of vapor-grown carbon nanofiber and polycarbonate composite sheets. *Mater. Lett.* **59,** 3514–3520 (2005).
22 Endo, M., Kim, Y. A., Hayashi, T., Nishimura, K., Matusita, T. & Miyashita, K. Vapor-grown carbon fibers (VGCFs)—Basic properties and their battery applications. *Carbon* **39,** 1287–1297 (2001).
23 Chung, D. D. L. Comparison of submicron-diameter carbon filaments and conventional carbon fibers as fillers in composite materials. *Carbon* **39,** 1119–1125 (2001).
24 Ghasemi, H., Carreau, P. J., Kamal, M. R. & Tabatabaei, S. H. Properties of PET/clay nanocomposite films. *Polym. Eng. Sci.* **52,** 420–430 (2012).
25 Dalir, H., Farahani, R. D., Nhim, V., Samson, B., Levesque, M. & Therriault, D. Preparation of highly exfoliated polyester-clay nanocomposites: process-property correlations. *Langmuir* **28,** 791–803 (2012).
26 Donadi, S., Modesti, M., Lorenzetti, A. & Besco, S. PET/PA Nanocomposite blends with improved gas barrier properties: effect of processing conditions. *J. Appl. Polym. Sci.* **122,** 3290–3297 (2011).

27 Nithikarnjanatharn, J., Ueda, H., Tanoue, S., Uematsu, H. & Iemoto, Y. Properties of polycarbonate/vapor grown carbon fiber composites prepared by melt compounding. *J. Text. Eng.* **57,** 97–106 (2011).
28 Mehdi, M., Mohammad, A., Uttandaraman, S. & Simon, P. The electrical conductivity and electromagnetic interference shielding of injection molded multi-walled carbon nanotube/polystyrene composites. *Carbon* **50,** 1455–1464 (2012).
29 Chen, D. Z., Yang, H. Y., He, P. S. & Zhang, W. A. Rheological and extrusion behavior of intercalated high-impact polystyrene/organomontmorillonite nanocomposites. *Compos. Sci. Technol.* **65,** 1593–1600 (2005).
30 Sadhu, S. & Bhowmick, A. K. Unique rheological behavior of rubber based nanocomposites. *J. Polm. Sci. Part B: Polym. Phys.* **43,** 1854–1864 (2005).
31 Muksing, N., Nithitanakul, M., Grady, B. P. & Magaraphan, R. Melt rheology and extrudate swell of organobentonite-filled polypropylene nanocomposites. *Polym. Test.* **27,** 470–479 (2008).
32 Yu, Z., Zhu, Z. Y. & Wang, S. Q. Synthesis and rheological properties of poly styrene/layered silicate nanocomposite. *Polymer* **46,** 3006–3013 (2005).
33 Hausnerova, B., Honkova, N., Lengalova, A., Kitano, T. & Saha, P. Rheology and fiber degradation during shear flow of carbon-fiber-reinforced polypropylene. *Polym. Sci. Ser. A* **48,** 951–960 (2006).
34 Kharchenko, S. B., Douglas, J. F., Obrzut, J., Grulke, E. A. & Migler, K. B. Flow-induced properties of nanotube-filled polymer materials. *Nat. Mater.* **3,** 564–569 (2004).
35 Xu, D. H., Wang, Z. G. & Douglas, J. F. Influence of carbon nanotube aspect ratio on normal stress differences in isotactic polypropylene nanocomposite melts. *Macromolecules* **41,** 815–825 (2008).
36 Cox, W. P. & Merz, E. H. Correlation of dynamic and steady-flow viscosities. *J. Polym. Sci.* **28,** 619–622 (1958).
37 Miyazono, K., Kagarise, C. D., Koelling Mahboob, M. & Bechtel, S. E. Shear and extensional rheology and flow-induced orientation of carbon nanofiber/polystyrene melt composites. *J. Appl. Polym. Sci.* **119,** 1940–1951 (2011).
38 Osaki, K., Murai, A., Bessho, N. & Kim, B. S. Linear viscoelastic relation concerning shear stresses at the strat and cessation of shear flow. *Nihon Reoroji Gakkaishi (J. Soc. Rheol. Jpn.)* **4,** 166–168 (1976).
39 Trouton, F. T. On the coefficient of viscous traction and its relation to that of viscosity. *Proc. R. Soc. Lond. A* **77,** 426–440 (1906).
40 Nielsen, J. K., Rasmussen, H. K., Hassager, O. & McKinley, G. H. Elongational viscosity of monodisperse and bidisperse polystyrene melts. *J. Rheol.* **50,** 453–476 (2006).
41 Bach, A., Almdal, K., Rasmussen, H. K. & Hassager, O. Elongational viscosity of narrow molar mass distribution polystyrene. *Macromolecules* **36,** 5174–5179 (2003).
42 Sugimoto, M., Koizumi, T., Taniguchi, T., Koyama, K., Saito, K., Nonokawa, D. & Morita, T. Melt Rheology of Hyperbranched-Polystyrene Synthesized with Multisite Macromonomer. *J. Polm. Sci. Part B: Polym. Phys.* **47,** 2226–2237 (2009).
43 Wagner, M. H., Kheirandish, S., Stange, J. & Munstedt, H. Modeling elongational viscosity of blends of linear and long-chain branched polypropylenes. *Rheol. Acta* **46,** 211–221 (2006).
44 Munstedt, H. Dependence of the elongational behavior of polystyrene melts on molecular weight and molecular weight distribution. *J. Rheol.* **24,** 847–867 (1980).
45 Shinohara, M. Uniaxial elongational viscosity of high molecular weight high density polyethylene melts. *Nihon Reoroji Gakkaishi (J. Soc. Rheol. Jpn.)* **19,** 118–124 (1991).
46 Batchelor, G. K. The stress generated in a non-dilute suspension of elongated particles by pure straining motion. *J. Fluid Mech.* **46,** 813–829 (1971).
47 Mewis, J. & Metzner, A. B. The rheological propertiesof suspensions of fibersin Newtonian fluids subjected to extensional defromations. *J. Fluid Mech.* **62,** 593–600 (1974).
48 Lubansky, A. S., Boger, D. V. & Cooper-White, J. J. Batchelor's theory extended to elongated cylindrical or ellipsoidal particles. *J. Non-Newtonian Fluid Mech.* **130,** 57–61 (2005).
49 Nithikarnjanatharn, J., Ueda, H., Tanoue, S., Uematsu, H. & Iemoto, Y. The rheological behavior and thermal conductivity of melt-compounded polycarbonate/vapor-grown carbon fiber composites. *Polym. J.* **44,** 427–432 (2012).
50 Takahashi, T., Takimoto, J. I. & Koyama, K. Uniaxial Elongational Viscosity of Various Molten Polymer Composites. *Polym. Compos.* **20,** 357–366 (1999).
51 Férec, J., Heuzey, M. C., Pérez-González, J., de Vargas, L., Ausias, G. & Carreau, P. J. Investigation of the rheological properties of short glass fiber-filled polypropylene in extensional flow. *Rheol. Acta.* **48,** 59–72 (2009).
52 Laun, H. M. Orientation effects and rheology of short glass fiber-reinforced thermoplastics. *Colloid Polym. Sci.* **262,** 257–269 (1984).
53 Chan, Y., White, J. L. & Oyanagi, Y. A fundamental study of the rheological properties of glass-fiber-reinforced polyethylene and polystyrene melts. *J. Rheol.* **22,** 507–524 (1978).
54 Jonathan, P. R. & Gareth, H. M. The axisymmetric contraction–expansion: the role of extensional rheology on vortex growth dynamics and the enhanced pressure drop. *J. Non-Newtonian Fluid Mech.* **98,** 33–63 (2001).
55 Bagley, E. B. & Birks, A. M. Flow of polyethylene into a capillary. *J. Appl. Phys.* **31,** 556–561 (1960).
56 Luo, X. L. & Mitsoulis, E. A numerical study of the effect of elongational viscosity on vortex growth in contraction flows of polyethylene melts. *J. Rheol.* **34,** 309–342 (1990).